Volume 6 | Number 40 | 28 October 2018 | Pages 19269–19864

Journal of Materials Chemistry A

Materials for energy and sustainability

rsc.li/materials-a

ISSN 2050-7488

ROYAL SOCIETY OF CHEMISTRY

PAPER

Johan Erlandsson, Lars Wågberg *et al.*

On the mechanism behind freezing-induced chemical crosslinking in ice-templated cellulose nanofibril aerogels

Journal of Materials Chemistry A

PAPER

View Article Online
View Journal | View Issue

Cite this: J. Mater. Chem. A, 2018, 6, 19371

On the mechanism behind freezing-induced chemical crosslinking in ice-templated cellulose nanofibril aerogels†

Johan Erlandsson, *[a] Torbjörn Pettersson, [ab] Tobias Ingverud, [be] Hjalmar Granberg, [c] Per A. Larsson, [ad] Michael Malkoch [e] and Lars Wågberg *[ab]

The underlying mechanism related to freezing-induced crosslinking of aldehyde-containing cellulose nanofibrils (CNFs) has been investigated, and the critical parameters behind this process have been identified. The aldehydes introduced by periodate oxidation allows for formation of hemiacetal bonds between the CNFs provided the fibrils are in sufficiently close contact before the water is removed. This is achieved during the freezing process where the cellulose components are initially separated, and the growth of ice crystals forces the CNFs to come into contact in the thin lamellae between the ice crystals. The crosslinked 3-D structure of the CNFs can subsequently be dried under ambient conditions after solvent exchange and still maintain a remarkably low density of 35 kg m^{-3}, *i.e.* a porosity greater than 98%. A lower critical amount of aldehydes, 0.6 mmol g^{-1}, was found necessary in order to generate a crosslinked 3-D CNF structure of sufficient strength not to collapse during the ambient drying. The chemical stability of the 3-D structure can be further enhanced by converting the hemiacetals to acetals by treatment with an alcohol under acidic conditions.

Received 2nd July 2018
Accepted 23rd August 2018

DOI: 10.1039/c8ta06319b

rsc.li/materials-a

Introduction

Nanocellulose aerogels have attracted great interest as a versatile platform for renewable functional materials. Aerogels have been used either as prepared, taking advantage of the inherent properties of cellulose nanofibrils (CNFs) such as lack of cytotoxicity[1] and creating tissue scaffolds,[2,3] or after post-functionalization, chemical or physical, to change or introduce new properties to the material making them useful as, for example, oil absorbents[4,5] and flexible devices.[6] However, a major shortcoming of nanocellulose aerogels is their lack of mechanical integrity when exposed to liquid water, in which they easily disintegrate. This limits their area of application, as well as the possibility of post-functionalization *via* water-based methods.[7,8] To overcome this, several chemical crosslinking strategies have been proposed that increase the structural integrity of nanocellulose aerogels. A common crosslinking procedure involves the addition of crosslinking agents to the nanocellulose prior to the fabrication of a dry material, through, for example, freeze-drying, where the crosslinking reaction can subsequently be thermally activated in the dry state.[2,9,10] The crosslinking of nanocellulose aerogels in the wet state has also been reported by using aldehyde-containing nanocellulose together with amine-containing crosslinkers,[11–14] as well as a simple cyclic freeze–thaw of TEMPO-oxidized CNFs.[15] Wet-stable aerogels made from highly charged CNFs have been developed into advanced functional materials by applying water-based modification methods such as the layer-by-layer technique,[16] and a variety of functional aerogels have been produced, including non-leaching antibacterial sponges, highly flame-retardant materials and 3-D interdigitated batteries and supercapacitors.[9,10,17]

A significant improvement in the resistance of cellulosic materials to moisture and water can be achieved by crosslinking induced by periodate oxidation. This oxidation selectively cleaves the C2–C3 bond in the 1,4-glucan unit[18] introducing aldehyde groups that can form crosslinks through inter-molecular and inter-particle hemiacetals by reacting with adjacent cellulose hydroxyls.[19,20] The formation of hemiacetal

[a]Division of Fibre technology, Department of Fibre and Polymer Technology, School of Engineering Sciences in Chemistry, Biotechnology and Health, KTH Royal Institute of Technology, Teknikringen 56, SE 100 44, Stockholm, Sweden. E-mail: jerland@kth.se; wagberg@kth.se

[b]Wallenberg Wood Science Center, KTH Royal Institute of Technology, Teknikringen 56, SE-100 44, 8 Stockholm, Sweden

[c]Papermaking & Packaging, Paper Technology, RISE Bioeconomy, Box 5064, SE-114-86, Stockholm, Sweden

[d]BiMaC Innovation, KTH Royal Institute of Technology, Teknikringen 8, SE-100 44, Stockholm, Sweden

[e]Division of Coating technology, Department of Fibre and Polymer Technology, School of Engineering Sciences in Chemistry, Biotechnology and Health, KTH Royal Institute of Technology, Teknikringen 56, SE-100 44, Stockholm, Sweden

† Electronic supplementary information (ESI) available. See DOI: 10.1039/c8ta06319b

bonds can be followed spectroscopically[20] but whether they act as crosslinks or not is however difficult to determine due to several possible reaction paths available for the formed aldehydes and the fact that the bond can form both intra- and intermolecularly.[19,21] Periodate oxidation has been applied to create highly porous and wet-stable lightweight materials based on nanocellulose, such as Pickering foams stabilized by modified CNFs.[22] Most recently, a facile method was reported for the production of wet-stable CNF aerogels without energy- and time-consuming freeze-drying and subsequent thermal activation of a crosslinker.[23] This procedure involved periodate oxidation, a freeze–thaw cycle and ambient drying after solvent exchange.[23] The resulting wet-stable CNF aerogels could be further functionalized with carbon nanotubes using the water-based layer-by-layer technique to introduce electrical conductivity. In addition, the functionalized aerogels were also used as electrodes in a supercapacitor and displayed a charge storage capacity of 9.8 F g^{-1}.[23] Indeed, the straightforward procedure has the potential to pave the way for scalable, faster and presumably easier production of functionalized CNF-based aerogels as it circumvents the use of crosslinking agents, freeze-drying and any post-activation of the crosslinking reaction. However, little attention has so far been devoted to studying the origin of the crosslinking reaction between aldehyde-containing CNFs and how the reaction parameters influence the final properties of aerogels. Additionally, no experiments, to the knowledge of the authors, have yet been performed to clarify the mechanisms behind the formation of the crosslinked 3-D structure and the influence of critical parameters on the aerogel preparation. The objective of the present work was therefore to study the properties of periodate-oxidized CNFs and the freezing-induced crosslinking mechanism, and also to investigate each part of the production procedure to distinguish the critical steps.

Materials and methods

Materials

Carboxymethylated CNFs were produced according to a previously reported method[24] and were provided by RISE Bioeconomy, Stockholm, Sweden, as a 20 g L^{-1} gel. Sodium metaperiodate, sodium chloride and hydroxylamine hydrochloride were purchased from Sigma Aldrich. Branched polyethylenimine (PEI) with a molecular weight of 60 kDa was purchased as a 50 wt% aqueous solution from Acros Organics (USA). Ethanol (96 vol%), ethylene glycol and acetone were purchased from VWR (Radnor, USA). All chemicals were used without further purification unless otherwise stated. MilliQ water with a resistivity of 18 MΩ was used throughout the experimental work.

Methods

Oxidation of cellulose nanofibrils. CNFs were oxidized by adding periodate to 20 g L^{-1} CNF gels, reaching final periodate concentrations of 7.5, 15, 30, 60 and 120 mM (the samples are hereafter referred to as Ox7.5, Ox15, Ox30, Ox60 and Ox120). The mixture was subsequently mixed with an Ultra Turrax (IKA Werke GmbH & Co. KG, Staufen, Germany) at 10 000 rpm for 5 min before the oxidation was continued without mixing or agitation for one hour in the absence of light to avoid photodegradation of the periodate as well as unwanted side-reactions.[25] The reaction was then quenched by the addition of a stoichiometric excess of ethylene glycol. After 2 h, the oxidized CNFs were washed exhaustively with water to remove remaining ethylene glycol and oxidation products from the quenching.

Cellulose nanofibril dispersions. Dispersions of carboxymethylated CNFs, *i.e.* without periodate treatment, were prepared according to an earlier described procedure,[26] where the original 20 g L^{-1} CNF-gel was diluted to 2 g L^{-1} and mixed in the Ultra Turrax for 10 min at 12 000 rpm. Following the mixing, 150 mL aliquots of the CNF dispersion were ultrasonicated using an ultrasonic probe (Sonics VCX 750, Newton, USA) at 300 W for 10 min. After sonication, the CNF dispersion was centrifuged for 1 h at 4500 rpm and the supernatant was collected for further use. The dry content of this supernatant was determined gravimetrically and compared with that of the original dispersion.

Dispersions of the periodate-oxidized CNFs were prepared by diluting the oxidized CNFs to the desired concentration, followed by Ultra Turrax mixing for 10 min at 12 000 rpm and ultrasonication for 30 min using an Elmasonic S15 sonication bath (Elma Schmidbauer GmbH, Singen, Germany), and finally filtration through a 5 μm syringe filter to remove any remaining aggregates. The oxidized CNF dispersions were used within twenty-four hours after their preparation.

Determination of the aldehyde content. The amount of aldehydes introduced into the CNFs by the periodate oxidation was determined by titration with sodium hydroxide after the reaction with hydroxylamine hydrochloride, which reacts with the aldehydes forming oximes while releasing a stoichiometric amount of protons.[21] The oxidized material was added to 25 mL of water containing 10 mM NaCl to ensure that the pH on the surface of the fibrils was the same as that in the bulk, and the pH was adjusted to 4. The sample mixture was then mixed with 25 mL of 0.25 M hydroxylamine hydrochloride solution (also containing 10 mM NaCl) adjusted to pH 4, and the mixture was allowed to react for 2 h after which the mixture was titrated back to pH 4 using 0.1 M NaOH. The amount of aldehydes in the sample was calculated from the number of moles of NaOH needed to reach pH 4, and the results were normalized with respect to the dry weight of the CNF sample.

Conductometric titration. Conductometric titration was used to determine the carboxyl content of the material and was performed with a Titrino 702 SM (Metrohm AG, Herisau, Switzerland) according to a previously described method.[27] Prior to the measurements, the CNF aerogels were washed with water to remove any trace amounts of salts remaining after the oxidation reaction. These aerogels were washed until the conductivity of the washing water was below 5 μS cm^{-1}. The carboxyl groups present in the materials were subsequently converted into their proton form by equilibration in water at pH 2 for 30 min after which they were again washed with water until the conductivity

of the water was below 5 μS cm^{-1}. Approximately 0.1 g of the CNF aerogel material (dry weight), carefully broken into small pieces, was added to a total volume of 500 mL of water containing 0.1 mM HCl and 2 mM NaCl. Nitrogen gas was bubbled through the solution for 15 min prior to the titration. The titration was performed with 0.1 M NaOH, and the amount of titrant used for calculation of the total charge was determined from the plateau region for the conductivity in the titration curve.[27]

Atomic force microscopy

Imaging. Atomic force microscopy (AFM) was used to examine CNFs adsorbed on plasma cleaned (3 min plasma cleaning, Harrick PDC-002, Harrick Scientific Corporation, USA) PEI-coated, silicon oxide surfaces (Si-Mat Silicon Materials, Germany) that had been activated in 0.1 M NaOH. The PEI was adsorbed by submersion for 5 minutes of the silicon surface in a 0.1 g L^{-1} PEI solution containing 10 mM NaCl, followed by excessive rinsing with MilliQ water containing 10 mM NaCl. CNFs were subsequently adsorbed from 0.1 g L^{-1} dispersions, also containing 10 mM NaCl, by submerging the substrate for 10 min followed by rinsing and drying in a flow of N_2 gas. The adsorbed CNFs were finally imaged in air using a Bruker Multimode 8 (Bruker, Santa Barbara, CA) run in the ScanAsyst mode with a cantilever having a nominal tip radius of 2 nm (SCANASYST-AIR, Bruker, Camarillo, CA).

Colloidal probe measurements. Colloidal probe AFM[28] measurements were performed on a symmetric (CNF–CNF) system to study the interaction forces between the CNFs in liquid, both on approach and separation. The interactions were monitored as a function of time in contact and of the chemical environment such as the salt concentration (0.1–10 mM NaCl) and pH (6.5–12). The chemical environment in the test cell was changed by injecting a new liquid while the surfaces were out of contact, and the system was then allowed to equilibrate before measurements were continued. For the analysis purpose, the concept of extended time in contact was chosen since it is difficult to determine exactly when the two surfaces come into contact. In AFM force measurements, it is possible to estimate the time in contact depending on experimental settings such as ramp velocity and trigger threshold, but the exact time in contact is also dependent on the response of the materials. The time in contact is dependent mainly on whether the materials are compressed on approach and also on the magnitude of the adhesive interaction. In the experiments, the contact time for the non-compressive and non-adhesive sample was approximately 0.5 s and the compression or adhesion increases the time in contact with up to approximately 0.3 s. The term of extended time in contact is therefore used, *i.e.* the prolonged time in contact at the highest applied load. The measurements were performed with a Veeco Instruments Multimode IIIa equipped with a Picoforce extension (Veeco Instruments Inc.), using a calibrated[29–31] CLFC-NOCAL tipless cantilever beam (Bruker, Camarillo, CA) with an attached SiO_2 particle (d = 5 μm, Thermo Scientific, USA). This SiO_2 particle was glued with Epikote 1009 (Shell Co) to the tipless beam ($L \times W$, 400 × 29 μm^2) using a manual micromanipulator under a reflective optical microscope. The deflection sensitivity used to convert the raw data to force as a function of separation was determined in measurements between the clean probe and the unmodified substrate.[32]

A simultaneous *in situ* modification of both the probe and substrate was carried out by sequentially adsorbing an anchoring layer of PEI from a 0.1 g L^{-1} PEI solution containing 10 mM NaCl for 5 min and CNFs from a dispersion for 20 min, with a washing step (10 mM NaCl solution) after each adsorption. The measurements were then performed by bringing the probe and surface into contact at a rate of 1 μm s^{-1}. Upon contact, defined as a measured force of 35 nN, the two surfaces were kept for an extended time in contact of 0, 10 or 60 s, after which the probe was retracted from the surface at a rate of 1 μm s^{-1}. The results were evaluated using AFM Force IT v2.6 (ForceIT, Järna, Sweden) software.

Preparation of crosslinked CNF aerogels by freeze-induced crosslinking

CNF aerogels were prepared by filling polystyrene Petri dishes with CNF dispersions containing sodium periodate (*i.e.* without the addition of ethylene glycol to quench the reaction), one hour after the initiation of the oxidation reaction. These Petri dishes were covered with lids to ensure that the CNF-periodate mixtures were tightly sealed, placed in a freezer (−20 °C) for two hours after which the frozen CNF samples were removed from the Petri dish and placed in acetone to thaw and solvent exchange. The acetone was replaced with fresh acetone every 15 min, repeated three times, before overnight drying of the samples under ambient conditions. These samples were stored dry until further analyses.

Scanning electron microscopy

The morphology of the produced aerogels was studied using an S-4800 field emission scanning electron microscope (SEM) (Hitachi, Tokyo, Japan). The aerogel samples were carefully cut and glued onto a sample holder using conductive carbon tape. Prior to imaging, these samples were coated with Pt/Pd in a Cressington 208HR sputter coater (Cressington Scientific Instruments, Watford, UK) for 40 s to limit specimen charging during SEM imaging. The pore size was quantified from SEM images as an average of the pore diameter measured in two perpendicular directions across the pore.

Mechanical testing of the CNF aerogels

The aerogels were tested on an Instron 5566 universal testing machine (Norwood, MA, USA) equipped with a 500 N load cell. The mechanical tests were performed to evaluate the wet-stability, *i.e.* indirectly assessing the amount of crosslinks in the materials. The samples consisted of cylindrical aerogel pieces, approximately 25 mm in diameter and approximately 15 mm thick (the exact dimensions were determined with a calliper before testing), which were soaked in water just before they were placed between two flat compression plates. The rate of compressive strain was 10% min^{-1}, and the samples were compressed until they reached 80% compression. The compressive strain rate was then reversed and relieved at the same rate

Table 1 Aldehyde contents and CNF diameters, from AFM measurements, of non-oxidized and CNFs oxidized with periodate concentrations of 7.5–120 mM

Sample	Analyzed aldehyde content (mmol g^{-1})	Average CNF diameter (nm)
No ox.	—	3.1 ± 0.7
Ox7.5	0.2 ± 0.2	3.2 ± 0.3
Ox15	0.35 ± 0.07	2.7 ± 0.8
Ox30	0.55 ± 0.07	2.9 ± 0.9
Ox60	0.7 ± 0	2.8 ± 0.9
Ox120	1.1 ± 0	3.3 ± 1

until 0% compression was reached. Each type of aerogel was tested in duplicate from two independent batches of aerogels.

Results

Aldehyde content and CNF morphology after periodate oxidation

As shown in Table 1, there was a continuous increase in the aldehyde content in the CNFs with the increasing periodate concentration during the oxidation, with the exception of the Ox7.5 and Ox15 which displayed an insignificant difference. Table 1 also shows the CNF diameter determined using AFM height-imaging and shows that the typical CNF diameter was 3.1 nm before oxidation, which corresponds well with earlier reported values,[33] and that the oxidation of the CNFs did not significantly affect their diameter. The diameter remained between 2.7 and 3.3 nm for all the oxidized samples.

Influence of periodate oxidation on CNF–CNF interactions studied with colloidal probe AFM

Colloidal probe AFM measurements were used to evaluate the direct interaction between oxidized CNFs and to test the hypothesis that crosslinking takes place between CNFs in the liquid, *i.e.* inter-CNF crosslinks are formed by hemiacetal bonds already in the compressed wet state. The interactions were studied for non-oxidized and Ox30 CNFs, both upon approach and on separation. Fig. 1A shows the adhesion forces for the Ox30 CNFs and the non-oxidized CNFs, where both CNF systems displayed increasing average adhesion forces with the increasing extended time in contact. The adhesive forces between the Ox30 CNFs were significantly greater than those between the non-oxidized CNFs: 2.3 ± 0.6 mN m^{-1}, 9.5 ± 2.3 mN m^{-1} and 12 ± 2.1 mN m^{-1} for the Ox30 CNFs at 0, 10 and 60 s extended time in contact, compared to 0.7 ± 0.2 mN m^{-1}, 1.3 ± 0.4 mN m^{-1} and 2.2 ± 0.4 mN m^{-1} for the non-oxidized CNFs.

A different trend was observed in the adhesion energy, shown in Fig. 1B, where the non-oxidized CNFs had a higher adhesion energy for the shortest extended time in contact (0 s), 5.3 ± 2.3 fJ, compared with 1.3 ± 1.2 fJ for the Ox30 CNFs. At 10 s extended time in contact, both CNF types had similar adhesion energies: 10.0 ± 2.8 fJ and 11.3 ± 4.4 fJ, respectively. At 60 s extended time in contact, the adhesion energy of the non-oxidised CNF system was significantly lower than that of the Ox30 CNF system, 18.4 ± 3.5 compared to 35.6 ± 9.0 fJ. Fig. 1C and D present separation curves of the Ox30 and the non-oxidized CNFs, respectively, where the distance of interaction for the Ox30 CNFs, 0–1000 nm, is shorter than that of the non-oxidized CNFs, 0–4000 nm. This is the major explanation for the higher adhesion energy of the non-oxidized CNF at the shortest contact time. Fig. 2 shows the AFM approach force curves, and the results for the non-oxidized CNFs are very different from those of the Ox30. Repulsive forces at distances of 1 μm and 400 nm in 0.1 mM and 10 mM NaCl were observed for the non-oxidized CNFs: a much longer distance than the 200 nm observed for the Ox30 CNFs in both 0.1 and 10 mM

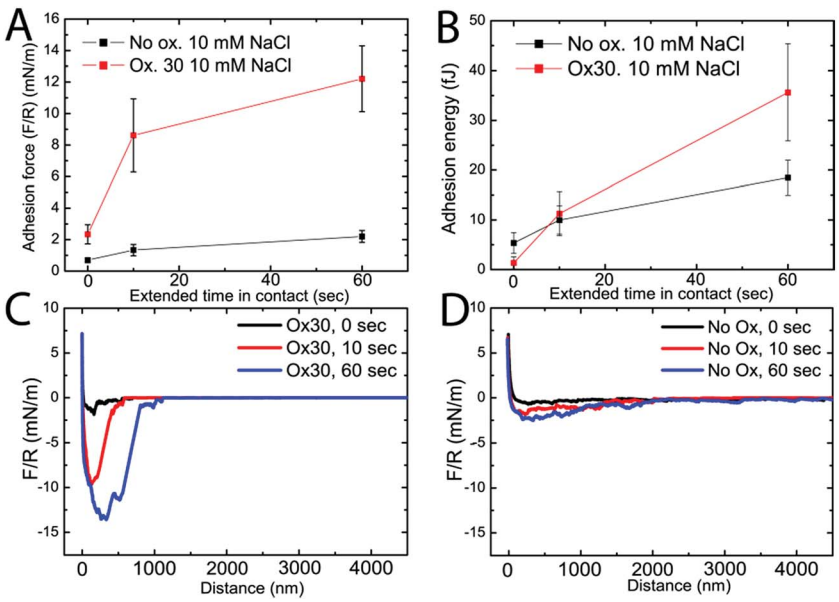

Fig. 1 (A) Normalized adhesion force (*F*/*R*) and (B) adhesion energy for the non-oxidized and Ox30 CNFs as a function of extended time in contact. (C) and (D) display separation curves for the Ox30 and non-oxidized CNFs respectively. Error bars are standard deviations ($n = 10$).

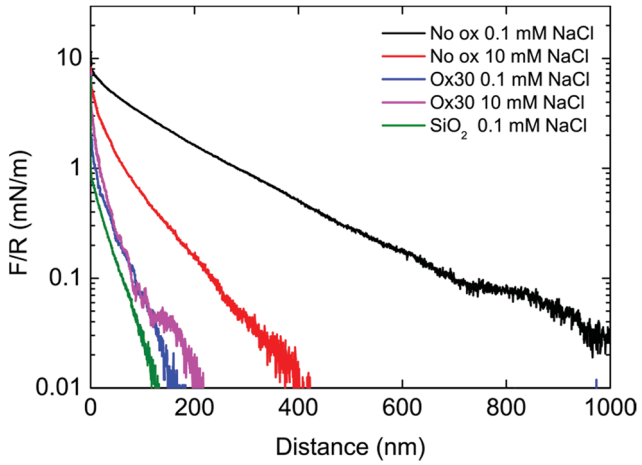

Fig. 2 Representative normalized force (F/R)–distance curves (upon approach) of non-oxidized CNFs and Ox30 CNFs in 0.1 and 10 mM NaCl.

NaCl. The distances at which repulsion began to be observed were much greater than the interaction distance between two clean silica surfaces, which was about 180 nm in 0.1 mM NaCl.

Since the formation, stability and reactions of hemiacetals are dependent on pH,[34] it follows that a change in pH would affect the adhesion between the CNFs if hemiacetal crosslinking was indeed present. Furthermore, if the aldehydes on the surface of the CNFs were reacted with a hydroxyl other than those on cellulose prior to bringing the surfaces into contact, inter-CNF crosslinks (between the two surfaces) would not be formed when the surfaces were brought together. The effect of changes in the chemical environment and treatment on the interactions between the CNFs was therefore studied, and Fig. 3 shows the effect of ionic strength and pH on the maximum adhesion force and adhesion energy between Ox30 CNFs.

As shown in Fig. 3, the adhesion force and adhesion energy followed the same pattern when conditions were changed, regardless of the extended time in contact. Both the adhesion force and adhesion energy displayed a reversible drop when the pH was increased from 6.5 to 12 and decreased back to 6.5, while keeping the background ionic strength constant. However, changing from pH 6.5 to EtOH (containing 0.1 M HCl) and back to pH 6.5 caused a larger and irreversible drop in both the adhesion force and adhesion energy that was unaffected by the extended time in contact. This indicates that the high adhesion force and high adhesion energy are indeed due to the

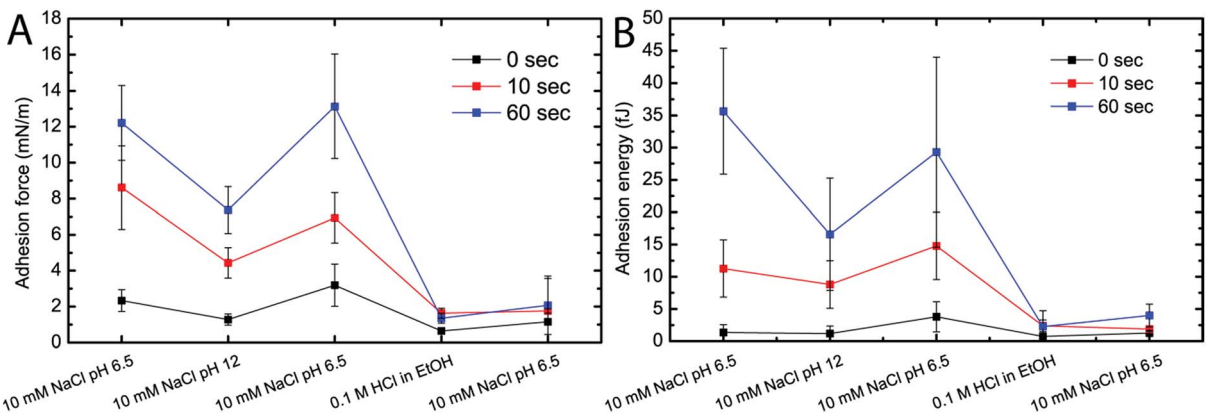

Fig. 3 (A) Normalised adhesion force (F/R) and (B) energy of adhesion between two Ox30 CNF surfaces at different extended times in contact as functions of A in the chemical environment. Error bars represent standard deviations ($n = 10$).

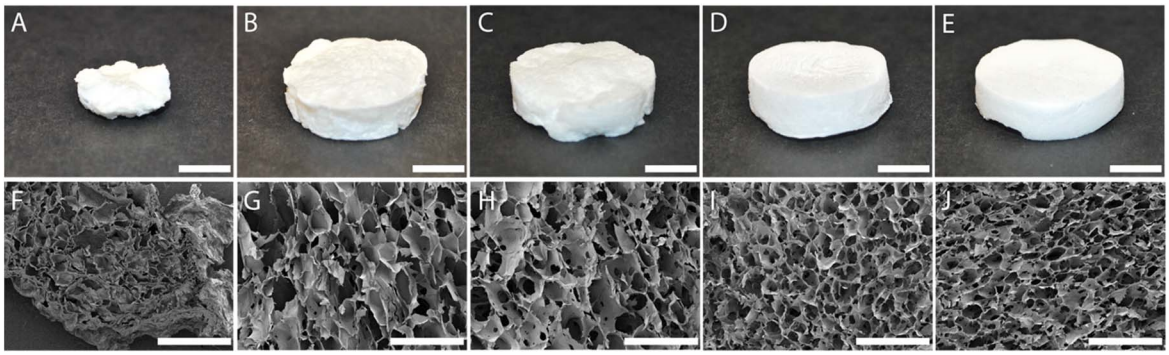

Fig. 4 The top row shows the photographs of solvent exchanged and dried samples made from (A) Ox7.5 CNFs, (B) Ox15 CNFs, (C) Ox30 CNFs, (D) Ox60 CNFs and (E) Ox120 CNFs; scale bars represent 10 mm. The bottom row (F–J) shows the SEM images of the cross sections of these samples; scale bars represent 1 mm.

Table 2 Pore diameter, apparent density, aldehyde content and total charge of the final wet-durable CNF aerogels: mean values with standard deviations

Sample	Ox7.5[a]	Ox15	Ox30	Ox60	Ox120
Pore diameter (μm)	164 ± 58	401 ± 155	391 ± 104	298 ± 77	224 ± 37
Density (kg m^{-3})	—	35 ± 1	35 ± 4	34 ± 2	37 ± 2
Aldehyde content (mmol g^{-1})	0.56 ± 0.02	0.6 ± 0.04	0.9 ± 0.3	1.23 ± 0.02	1.9 ± 0.06
Total charge (mmol g^{-1})	0.64 ± 0.04	0.62 ± 0.01	0.60 ± 0.08	0.60 ± 0.08	0.64 ± 0.1

[a] Ox7.5 was not considered to be an aerogel.

formation of hemiacetals between the cellulose surfaces in aqueous media.

Structure and aldehyde content of CNF aerogels

The sequential procedure of periodate oxidation, freezing, thawing in acetone, a solvent exchange and drying under ambient conditions resulted in stable aerogels from the Ox15, Ox30, Ox60 and Ox120 CNFs, but not from the Ox7.5 CNFs which displayed a large collapse on drying. Fig. 4 shows the macroscopic (top panel) and the microscopic (bottom panel) structures of the dry samples. The Ox15–Ox120 samples were able to withstand the evaporation of the solvent without collapse and formed aerogels with porosities greater than 98%.

The Ox60 and Ox120 CNFs formed aerogels with a macroscopically smoother surface than Ox30 and Ox15 CNFs. In addition, the pore structure was found to be more regular and the pores were smaller (Fig. 4F–J) when the periodate concentration increased. The lamellae (pore walls) formed (Fig. S1, in the ESI†) were shown to consist of CNFs that had been pressed tightly together by growing ice crystals during the aerogel fabrication process, forming an open-cell structure.[35] From the SEM images, it was estimated that the typical thickness of the lamellae was 800 nm. The chemical and physical properties of the aerogels are listed in Table 2.

The average pore diameter decreased from 401 μm to 224 μm with increasing the periodate concentration from 15 mM to 120 mM while the density of the aerogels remained unaffected and was constant at approximately 35 kg m^{-3}. The total charge also remained constant, *i.e.* the carboxylic acid content introduced by the carboxymethylation had a stable value of *ca.* 0.6 mmol g^{-1}. On the other hand, the aldehyde content in the final aerogels steadily increased, from 0.56 mmol g^{-1} to 1.9 mmol g^{-1}, when the periodate concentration was increased.

Mechanical properties

Wet mechanical testing has been reported as an indirect method for assessing the presence of crosslinks in CNF aerogels.[23] Fig. 5A shows stress–strain curves of water-soaked aerogels, and all the materials except those made from Ox7.5 CNFs displayed similar mechanical properties, regardless of the periodate concentration used. All the aerogels displayed a significant shape recovery of approximately 70% when the compressive load was released. Such a behaviour is in line with earlier reported studies on chemically crosslinked CNF aerogels.[9,23] Notably, shape recovery, after compression, was completely absent in the non-oxidized CNF materials, which also displayed a decrease in stress due to sample failure at a compressive strain of about 35%.

To identify the preparation steps necessary for the creation of sufficient inter-CNF crosslinks and for the formation of a wet-stable aerogel, the mechanical properties were investigated for samples made according to slightly different preparation procedures. The parameters investigated were the freezing temperature and the use of solvent exchange, using Ox60 CNFs. Fig. 5B shows stress–compression curves for Ox60 CNF samples produced with different procedures. Both the non-solvent-

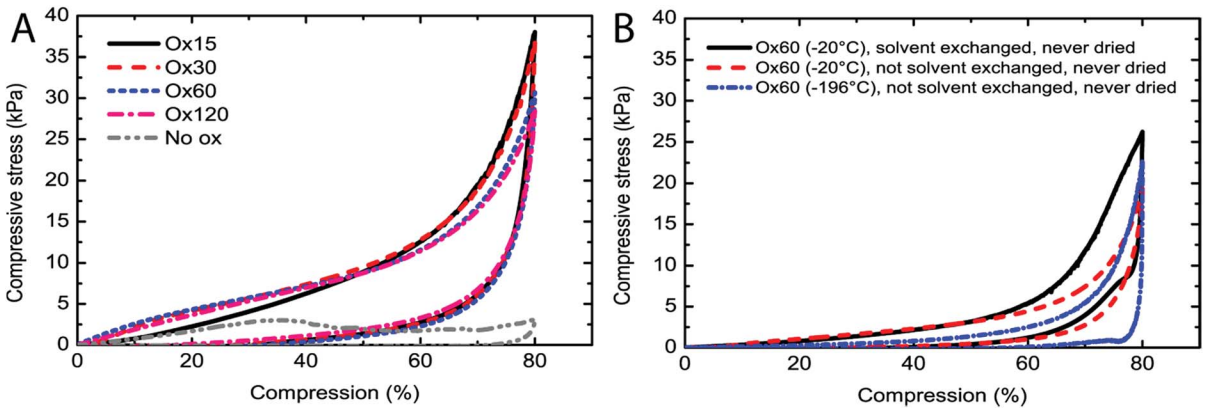

Fig. 5 (A) Stress–compression curves of Ox15–Ox120 CNF aerogels soaked in water just prior to the compression test. No ox. is a sample made from non-oxidized CNFs. (B) Stress–compression curves of never-dried Ox60 CNF "aerogels" made using different fabrication procedures.

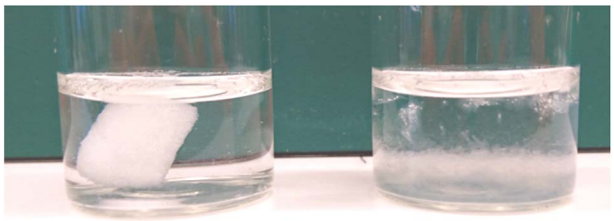

Fig. 6 Photographs taken 30 min after immersion of two Ox60 CNF aerogel pieces in water at pH 12. The piece to the left had been treated in 0.1 M HCl ethanol for 30 min, before being washed with water. The sample to the right was a pristine Ox60 CNF aerogel without further acid and ethanol treatment.

exchanged and the solvent-exchanged Ox60 CNF aerogels (−20 °C) displayed the characteristic compression curve of a crosslinked CNF material with a shape recovery of 60%. In contrast, the Ox60 CNF "aerogels" formed by rapid freezing in liquid nitrogen (−196 °C), and kept there for two hours before thawing without any solvent exchange, were weaker under compression. These weak structures fractured during compression and showed no shape recovery. Of the two Ox60 aerogels formed at −20 °C, the one that was solvent exchanged to acetone and back to water had the highest mechanical strength at 80% compression.

Chemical stability of the crosslinked aerogels

To further explore the presumed crosslinking by hemiacetals, the samples of Ox60 CNF aerogels were subjected to the same changes in the chemical environment as the CNFs in the colloidal probe AFM measurements. If the crosslinking reaction was prevented from taking place, reversed or enhanced due to the changes in aerogel treatment, the aerogel properties would be ultimately affected. Fig. 6 shows two pieces of the Ox60 CNF aerogel placed in water at pH 12, one with no further treatment after solvent exchange and the other further treated with ethanol containing 0.1 M HCl. Note that under acidic ethanol conditions no significant adhesive force was observed upon bringing two surfaces together, but in the aerogel they were already in contact when the conditions were changed. The non-ethanol-treated aerogel disintegrated completely, without agitation, within one minute after immersion in water adjusted to pH 12, whereas the ethanol/HCl-treated aerogel remained intact for several hours under the same conditions, even after vigorous agitation.

Discussion

Oxidation of the CNFs

An increasing dosage of periodate during oxidation produced CNFs with increasing aldehyde contents, ranging from 0.2 to 1.1 mmol g^{-1}. This increasing trend is in agreement with earlier studies on oxidation of nanocellulose.[19,36,37] These aldehyde contents were lower than those in the corresponding aerogels, (see Tables 1 and 2) which indicate that oxidation continues in the freezer. Considering the relatively low aldehyde content in the non-frozen CNFs, given that the maximum is 12.5 mmol g^{-1}, and that other oxidations, such as TEMPO-mediated oxidation, have been reported to be limited to the surface C6-carbons of the CNFs, where complete oxidation of all C6 carbons corresponds to 1.7 mmol carboxyl groups per gram of cellulose,[38] it is suggested that the periodate oxidation of the CNFs at the degree of oxidation here studied was also in principle confined first to the surface of the fibril aggregates and then to the surface of the single fibrils.[19,39] Complete oxidation of all the cellulose on the CNF surface gives an aldehyde content of 3.4 mmol g^{-1} as two aldehydes are generated per C2–C3 bond. This is supported by the retained dimensions of the CNFs, since only higher degrees of oxidation drastically changed the dimensions of the oxidized CNFs,[19] causing them to decrease in size. In addition, the fraction of accessible C2–C3 bonds on the surface can be calculated[38] and subsequently also the surface density of aldehydes by using the measured dimensions of the fibrils and the alternating arrangement of the anhydroglucopyranose units in the cellulose chains in the crystal structure.[40] None of the Ox7.5–Ox120 systems have fibril surfaces saturated with aldehydes. In the Ox120 CNFs, which had the highest aldehyde content, only 68% of all the accessible C2–C3 bonds on the CNF surface was oxidized, corresponding to 0.78 groups per nm^2. These observations and calculations suggest that under the reaction conditions and times used here, periodate oxidation was predominantly limited to the surface of the CNFs, but inhomogeneities may naturally occur.

Effect of periodate oxidation on interactions between the CNFs

Considerably greater adhesion forces (Fig. 1A) were observed between the Ox30 CNFs than between the non-oxidized CNFs, and the adhesion force was strongly dependent on the extended time in contact. An extension of the time in contact naturally allows more time for the CNFs to interact and form, for example, entanglements or chemical bonds, which would result in greater adhesion forces. The density and surface morphology of both CNF types are approximately the same (Fig. S2, in the ESI†), which means that it is not the amount of material or its morphology that causes the differences. The greater adhesion is therefore suggested to be related to the chemistry of the CNFs and to the ability of the modified CNFs to form chemical bonds. In support of the different interaction mechanisms are also the origin and development of the adhesion energy with an extended time in contact (Fig. 1B). The non-oxidized CNFs, without aldehydes, displayed a long-distance interaction behaviour typically observed in systems such as polyelectrolyte multilayer films that have a high propensity to form entanglements (Fig. 1D).[41] This was observed as a jagged pattern in the force curve. The Ox30 CNFs displayed a less jagged interaction behaviour (Fig. 1C) and distinct snap-off behaviour at a shorter separation, indicating less surface entanglement. It is therefore suggested that the energy of adhesion of the non-oxidized CNFs is related to entanglements and weak interactions over a longer interaction distance and that the energy of adhesion of the Ox30 CNFs is related to the strong crosslinks between CNFs. The shorter interaction distance, lack of entanglements, different response

and higher energy of adhesion after a longer extended time in contact strongly suggests that the CNFs are held together by chemical bonds rather than physical entanglement and that it requires some time to achieve an intimate contact between the fibrils. The significantly shorter distances over which the Ox30 CNFs interact on approach (Fig. 2) also indicate that the adsorbed Ox30 CNF films are more rigid and that they do not extend from the surface, whereas the non-oxidized CNFs extend from the surface. The extension from the surface causes electrosteric repulsive forces to be observed at distances of 1000 nm and 400 nm in 0.1 mM and 10 mM NaCl, respectively. This response to ionic strength resembles that of a swelling and de-swelling of a polyelectrolyte gel.[42] The Ox30 CNFs are almost unaffected by a change in ionic strength, and they display repulsive forces at approximately 200 nm in both 0.1 mM and 10 mM NaCl, which can be explained by the crosslinking between the CNFs even within the adsorbed film, where the CNFs are brought into close contact by attractive forces created by the pre-adsorbed PEI. These forces are naturally the same for the non-oxidized CNF, as the charge of the CNFs is unaffected by the oxidation, but the aldehydes obviously create an additional interaction and eventually form crosslinks, expressed by the shorter interaction distance. A less swollen state of the Ox30 CNFs was observed in QCM-D measurements (Fig. S3 of the ESI†), where the Ox30 CNFs displayed characteristics of a less extended film than a film of non-oxidized CNFs. The higher ionic strength during the periodate treatment naturally allows for a closer contact between the fibrils, but the irreversibility of this compaction, detected upon rinsing, indicates that additional interactions are effective during the periodate treatment.

Origin of the crosslinks between the periodate oxidized CNFs

It has often been reported that both intra- and intermolecular hemiacetal bonds are readily formed from aldehydes introduced by periodate oxidation and hydroxyls in cellulose.[19,43] In order to evaluate the formation of such bonds between the CNFs in this work, the chemical conditions were changed to favour, inhibit or completely block their formation. Fig. 3 shows the adhesion force and the adhesion energy when the chemical conditions were changed. When the pH was increased from 6.5 to 12, at a constant ionic strength (10 mM), both the adhesion force and energy decreased. Since it is known that hemiacetals are not formed at high pH values and that they break if already formed because the equilibrium is shifted to the free aldehyde and alcohol functionalities,[34] it is suggested that the overall decrease in adhesion is due to a failure to maintain covalent hemiacetal bonds between the fibrils. This hypothesis is strengthened by the fact that the inhibited interaction is reversible and that the overall adhesion increased when the pH was reduced to 6.5, *i.e.* back to the condition where hemiacetals are readily formed. The formation of inter-surface crosslinks, before the surfaces were brought together, was blocked by treating the Ox30 CNF surfaces with an acidic ethanol solution, when "free" aldehydes from the periodate oxidation will predominantly form hemiacetals with ethanol instead of cellulose. The hemiacetals formed with ethanol might possibly also continue to form acetals and thus completely eliminate the possibility of hemiacetal formation between fibrils when the surfaces are brought into contact. If the strong adhesion observed is due to hemiacetals, this treatment should decrease the adhesion, as was indeed shown to be the case (Fig. 3). The "blocking" treatment resulted in an irreversible reduction in adhesion energy and adhesion force, which indicate the formation of pH-stable acetals with ethanol under acidic conditions. It is therefore suggested that hemiacetals are formed between periodate-oxidized CNFs under neutral conditions where "free" aldehydes are available on the surface of the CNFs and also possibly through the rearrangement of hemiacetals. An increase in pH shifts the reaction to free aldehydes and hydroxyls, resulting in fewer hemiacetals formed between individual CNFs and consequently a weaker adhesion between the surfaces. When the aldehydes were completely blocked by the formation of acetals by, for example, a reaction with ethanol, the adhesion was irreversibly lowered, as no covalent bonds could then form between the two surfaces.

The chemical stability of the CNF aerogels agrees well with the AFM results obtained with the colloidal probe technique. The reaction equilibrium shifted at high pH values, causing the aerogel to easily disintegrate. This disintegration is attributed to the break-up of the hemiacetal bonds holding the structure together. The increased stability after treatment with acid and ethanol is attributed to a conversion of the already present hemiacetals into acetals which, in contrast to hemiacetals, are stable under alkaline conditions.

Effect of periodate concentration on the formation and properties of the crosslinked CNF aerogels

Aldehyde-containing CNFs clearly display a higher adhesion energy than their non-aldehyde containing counterparts when they come into close contact. In Fig. 4F–J, all the samples clearly display pore structures where the CNFs have been compressed into dense lamellae, *i.e.* a structure that would enable the oxidized CNFs to crosslink. The effects of the periodate concentration during the oxidation of the CNFs, *i.e.* the aldehyde content, on the properties and the ability of the CNFs to form water-durable aerogels by the sequential oxidation, freezing–thawing, solvent exchange and ambient drying are therefore of interest. A noticeable effect of an increase in the periodate concentration was the increase in the macroscopic smoothness of the aerogels (Fig. 4A–E), probably because both Ox60 and Ox120 CNFs were, qualitatively, less viscous than the Ox15 and Ox30 CNFs, which facilitated a better filling of the moulds. The less viscous behaviour of the Ox60 and Ox120 was similar to previous observations of CNFs together with monovalent salts.[46] The decreasing average pore size for the Ox15–Ox120 aerogels is also in agreement with earlier observations, where an increase in the salt concentration has been reported to decrease the size of the ice crystals formed upon freezing.[44] The bulk densities of the aerogels were not significantly affected by the periodate concentration used during oxidation, *i.e.* by the aldehyde content of the CNFs, and given that the amount of the dry material was the same and that the crosslinking of the

structure was strong enough to withstand shrinkage, similar aerogel densities were indeed expected.

It is suggested that the ability to withstand shrinkage during drying is linked to the amount of crosslinks in the aerogel. Clearly, since the Ox7.5 sample collapsed (Fig. 4), the amount of aldehydes introduced into this system after freezing (0.56 mmol g^{-1}) was not sufficient to form a structure strong enough to withstand the drying. However, since the Ox15 CNFs, with an aldehyde content of 0.6 mmol g^{-1} after freezing, were able to withstand the drying, there seems to be a narrow region determining whether or not the structure formed is able to withstand drying. In the case of drying from acetone, an amount in excess of 0.6 mmol g^{-1} was not necessary to achieve a crosslinked, non-collapsing CNF network. This is supported by the fact that the Ox15–Ox120 CNF aerogels all displayed similar mechanical properties (Fig. 5A) with a good shape recovery in the wet state, similar to that of earlier reported hemiacetal-crosslinked CNF aerogels,[23] even though it would be possible to achieve a more crosslinked system in systems with a higher aldehyde content. However, for a surface-limited oxidation and the formation of hemiacetals between surface aldehydes and surface hydroxyls, the degree of crosslinking is dependent on the presence of both groups. As the aldehyde content increases, the hydroxyl content decreases (assuming that the aldehydes can form hemiacetals with all hydroxyl groups of cellulose and not only the C6 groups), and this decreases the rate of the crosslinking reaction. This is supported by studies performed on periodate-oxidized pulp fibres, where an increase in the quantity of free aldehydes was observed as an increase in the carbonyl peak at 1740 cm^{-1} with increasing oxidation, suggesting that the aldehydes do not participate in other chemical bonds.[45]

Effect of freezing and solvent exchange on the formation of crosslinked aerogels

The crucial steps in the creation of crosslinked CNF aerogels were identified by mechanical tests of the Ox60 CNF aerogels (Fig. 5B) made using different freezing temperatures and drying after solvent exchange to acetone. The two samples that were frozen slowly at −20 °C, one thawed in water and one in acetone, displayed stress–strain curves characteristic of a crosslinked material, *i.e.* with a significant shape recovery, whereas the sample rapidly frozen at −196 °C did not form a stable aerogel but fractured during compression and completely lacked shape recovery. None of these samples were completely dried before testing, which suggests that neither drying nor solvent exchange is crucial for the crosslinking of the CNFs, since the sample without solvent exchange also appeared to be crosslinked. The frozen-only sample, *i.e.* the sample that was not solvent-exchanged, was slightly weaker than the solvent-exchanged aerogel, which can be expected since water is a known plasticizer for cellulose. The solvent exchange apparently contributed only to the final strength of the CNF aerogel, and the sample that was not solvent exchanged was plasticized with water. The greater strength of the solvent-exchanged sample is probably only temporary, as it takes time for water to penetrate the crosslinked structure, as was observed earlier.[23] This delayed plasticizing effect of CNF aerogels has been reported earlier.[23] Interestingly, too rapid a freezing did not produce as strong CNF networks as slow freezing. The reason for the lack of crosslinking after rapid freezing is attributed to the lack of time for the CNFs to form bonds and crosslink during the rapid cooling. Faster cooling also prevents the CNFs from being properly packed together, which was shown in the AFM study to be important for hemiacetal formation. Both poor packing and low temperature probably slow down the crosslinking kinetics, preventing the formation of a sufficient number of bonds between the CNFs, and a non-crosslinked CNF structure is produced. The observed continued oxidation in the freezer suggests that chemical reactions may proceed even though the structure appears to be frozen. It should be noted that the ionic strength of the water front escaping from ice crystals together with the fibrils is probably very high, preventing the water front from freezing until a sufficiently low temperature is reached.

Conclusions

This study provides insight into the periodate oxidation of CNFs and the ability of oxidized CNFs to subsequently form crosslinked aerogels by freeze-linking, a freezing-induced crosslinking reaction, by the formation of crosslinks in the form of hemiacetals or even acetals. The interactions between individual CNFs change dramatically after oxidation, and the oxidized CNFs interact at significantly shorter distances than non-oxidized CNFs. These shorter distances are due to the higher adhesion forces between the oxidized CNFs within the film, because crosslinks formed between CNFs prevent the CNFs from extending from the surface. The underlying adhesion mechanism of the oxidized system was revealed to be different from that of the non-oxidized system where CNFs adhere mostly through entanglements while the oxidized CNFs adhere mainly through short-range chemical bonds. Inter-CNF bonds between oxidized CNFs are readily formed when the CNFs are pressed together, which would occur during freezing, where the CNFs and the ice phase separate and the CNFs are tightly packed in a lamellar structure in-between the ice crystals under considerable pressure, *i.e.* an ice-templated structure. Bonding would also occur in the tightly adsorbed layers during the colloidal probe AFM measurements when two surfaces of oxidized CNFs are pressed together. It is also suggested that the chemical bonds formed between the CNFs are predominantly hemiacetal bonds, which was demonstrated by changing the chemical environment to either favour or inhibit their formation. As an example, the inter-CNF hemiacetal formation can be inhibited by an increase in pH and completely blocked by, for example, treating the oxidized CNFs with ethanol under acidic conditions, *i.e.* conditions under which hemiacetal and possibly acetal bonds can be formed together with ethanol. The chemical stability of the aerogels was also enhanced by an acidic ethanol treatment, which also supports the hypothesis that stable acetal bonds are present. The densities and the mechanical properties of the aerogels fabricated were unaffected by the periodate concentration, but the pore size of the aerogels can be tuned by changing the ionic strength of the gel

before freezing; a critical amount of aldehydes (0.6 mmol g^{-1}) is needed in order to create a structure with enough crosslinks to be able to withstand ambient drying of an acetone-soaked aerogel. It was also demonstrated that a slow freezing step is crucial for the production of hemiacetal-crosslinked CNF aerogels, where the growing ice crystals squeeze the CNFs together into a tightly packed structure forming the pore walls where the oxidation continues, and the aldehydes formed are then able to form hemiacetal bonds that crosslink the CNFs.

Conflicts of interest

There are no conflicts to declare.

Acknowledgements

The authors gratefully acknowledge the Swedish Energy Agency for funding through Batterifonden and the MODULIT-project (grant number 37716-1). L. Wågberg, T. Pettersson and T. Ingverud acknowledge the Wallenberg Wood Science Center, and P. A. Larsson acknowledges the BiMaC Innovation Centre at KTH for financial support. Michael Malkoch acknowledges the Knut and Alice Wallenberg foundation for financial support.

Notes and references

1 L. Alexandrescu, K. Syverud, A. Gatti and G. Chinga-Carrasco, *Cellulose*, 2013, **20**, 1765.
2 H. Cai, S. Sharma, W. Liu, W. Mu, W. Liu, X. Zhang and Y. Deng, *Biomacromolecules*, 2014, **15**, 2540.
3 C. Zhang, T. Zhai and L.-S. Turng, *Cellulose*, 2017, **24**, 2791.
4 N. Cervin, C. Aulin, P. Larsson and L. Wågberg, *Cellulose*, 2012, **19**, 401.
5 J. Feng, S. T. Nguyen, Z. Fan and H. M. Duong, *Chem. Eng. J.*, 2015, **270**, 168.
6 M. S. Toivonen, A. Kaskela, O. J. Rojas, E. I. Kauppinen and O. Ikkala, *Adv. Funct. Mater.*, 2015, **25**, 6618.
7 C. H. Kim, H. J. Youn and H. L. Lee, *Cellulose*, 2015, **22**, 3715–3724.
8 W. Zhang, Y. Zhang, C. Lu and Y. Deng, *J. Mater. Chem.*, 2012, **22**, 11642.
9 M. Hamedi, E. Karabulut, A. Marais, A. Herland, G. Nyström and L. Wågberg, *Angew. Chem., Int. Ed.*, 2013, **52**, 12038.
10 G. Nyström, A. Marais, E. Karabulut, L. Wågberg, Y. Cui and M. M. Hamedi, *Nat. Commun.*, 2015, **6**, 7259.
11 K. Syverud, H. Kirsebom, S. Hajizadeh and G. Chinga-Carrasco, *Nanoscale Res. Lett.*, 2011, **6**, 1.
12 K. Syverud, S. R. Pettersen, K. Draget and G. Chinga-Carrasco, *Cellulose*, 2015, **22**, 473.
13 J. Lindh, C. Ruan, M. Strømme and A. Mihranyan, *Langmuir*, 2016, **32**, 5600.
14 X. Yang and E. D. Cranston, *Chem. Mater.*, 2014, **26**, 6016.
15 F. Jiang and Y.-L. Hsieh, *J. Mater. Chem. A*, 2014, **2**, 350.
16 G. Decher, *Science*, 1997, **277**, 1232.
17 J. Henschen, J. Illergård, P. A. Larsson, M. Ek and L. Wågberg, *Colloids Surf., B*, 2016, **146**, 415.
18 E. L. Jackson and C. S. Hudson, *J. Am. Chem. Soc.*, 1937, **59**, 2049.
19 N. Guigo, K. Mazeau, J.-L. Putaux and L. Heux, *Cellulose*, 2014, **21**, 4119.
20 A. Codou, N. Guigo, L. Heux and N. Sbirrazzuoli, *Compos. Sci. Technol.*, 2015, **117**, 54.
21 H. Zhao and N. Heindel, *Pharm. Res.*, 1991, **8**, 400–402.
22 N. T. Cervin, E. Johansson, P. A. Larsson and L. Wågberg, *ACS Appl. Mater. Interfaces*, 2016, **8**, 11682.
23 J. Erlandsson, V. López Durán, H. Granberg, M. Sandberg, P. A. Larsson and L. Wågberg, *Appl. Mater. Today*, 2016, **5**, 246.
24 L. Wågberg, G. Decher, M. Norgren, T. Lindström, M. Ankerfors and K. Axnäs, *Langmuir*, 2008, **24**, 784.
25 F. S. H. Head and H. A. Standing, *J. Chem. Soc.*, 1952, 1457, DOI: 10.1039/JR9520001457.
26 A. B. Fall, A. Burman and L. Wågberg, *Nord. Pulp Pap. Res. J.*, 2014, **29**, 176.
27 S. Katz, R. Beatson and A. M. Scallan, *The determination of strong and weak acidic groups in sulfite pulps*, 1984.
28 W. A. Ducker, T. J. Senden and R. M. Pashley, *Nature*, 1991, **353**, 239.
29 E. Thormann, T. Pettersson and P. M. Claesson, *Rev. Sci. Instrum.*, 2009, **80**, 093701.
30 J. E. Sader, J. W. M. Chon and P. Mulvaney, *Rev. Sci. Instrum.*, 1999, **70**, 3967.
31 T. Pettersson, N. Nordgren, M. W. Rutland and A. Feiler, *Rev. Sci. Instrum.*, 2007, **78**, 093702.
32 T. Pettersson and A. Dėdinaitė, *J. Colloid Interface Sci.*, 2008, **324**, 246.
33 A. B. Fall, S. B. Lindström, O. Sundman, L. Ödberg and L. Wågberg, *Langmuir*, 2011, **27**, 11332.
34 T. J. Przystas and T. H. Fife, *J. Am. Chem. Soc.*, 1981, **103**, 4884.
35 P. Munier, K. Gordeyeva, L. Bergström and A. B. Fall, *Biomacromolecules*, 2016, **17**, 1875.
36 U.-J. Kim, S. Kuga, M. Wada, T. Okano and T. Kondo, *Biomacromolecules*, 2000, **1**, 488.
37 J. Wu, Y. Zheng, Z. Yang, Q. Lin, K. Qiao, X. Chen and Y. Peng, *RSC Adv.*, 2014, **4**, 3998.
38 Y. Okita, T. Saito and A. Isogai, *Biomacromolecules*, 2010, **11**, 1696.
39 A. Sjöstedt, J. Wohlert, P. T. Larsson and L. Wågberg, *Cellulose*, 2015, **22**, 2943.
40 Y. Nishiyama, P. Langan and H. Chanzy, *J. Am. Chem. Soc.*, 2002, **124**, 9074.
41 T. Pettersson, S. A. Pendergraph, S. Utsel, A. Marais, E. Gustafsson and L. Wågberg, *Biomacromolecules*, 2014, **15**, 4420.
42 Z. Feldötö, T. Pettersson and A. Dėdinaitė, *Langmuir*, 2008, **24**, 3348.
43 J. Lindh, D. O. Carlsson, M. Strømme and A. Mihranyan, *Biomacromolecules*, 2014, **15**, 1928.
44 S. Wu, C. Zhu, Z. He, H. Xue, Q. Fan, Y. Song, J. S. Francisco, X. C. Zeng and J. Wang, *Nat. Commun.*, 2017, **8**, 15154.
45 V. López Durán, P. A. Larsson and L. Wågberg, *Cellulose*, 2016, **23**, 3495.
46 A. Naderi and T. Lindström, *Cellulose*, 2014, **21**, 3507–3514.

